

<sup>8</sup>D. von Ehrenstein and J. P. Schiffer, Phys. Rev. **164**, 1374 (1967).

<sup>9</sup>H. Bertschat, U. Leithäuser, K. H. Maier, E. Recknagel, and B. Spellmeyer, to be published.

<sup>10</sup>H. Noya, A. Arima, and H. Horie, Progr. Theor. Phys., Suppl. No. 8, 33 (1958).

<sup>11</sup>T. P. Das and M. Pomerantz, Phys. Rev. **123**, 2070 (1961).

<sup>12</sup>N. C. Mohapatra, C. M. Singal, and T. P. Das, Phys. Rev. Lett. **31**, 580 (1973).

<sup>13</sup>Interpolated lattice parameters for Zn: *Gmelins Handbuch der anorganischen chemie, Zink, Ergänzungsband* (Verlag Chemie, Weinheim, Germany, 1956), p. 282. Interpolated lattice parameters for Cd: *ibid.*, *Cadmium, Ergänzungsband* (Verlag Chemie, Weinheim, Germany, 1959), p. 56.

## Electroproduction of $K^+$ Mesons in the Forward Direction\*

C. J. Bebek, C. N. Brown, M. Herzlinger, S. Holmes, C. A. Lichtenstein, F. M. Pipkin,  
and L. K. Sisterson

*Cyclotron Laboratory, Harvard University, Cambridge, Massachusetts 02138*

and

D. Andrews,† K. Berkelman, D. G. Cassel, and D. L. Hartill  
*Laboratory of Nuclear Studies, Cornell University, Ithaca, New York 14850*

and

N. Hicks

*Wellesley College, Wellesley, Massachusetts 02181*

(Received 23 October 1973)

We present data on electroproduction of  $K^+$  mesons off protons. Measurements were made at data points with nominal  $(Q^2, W)$  values of (0.6, 2.67), (1.2, 2.67), (2.0, 2.67), and (1.2, 2.15) in  $(\text{GeV}^2, \text{GeV})$ . The virtual photoproduction cross section for  $K^+ + \text{MM}$  is studied as a function of missing mass,  $x'$ ,  $P_{\perp}^2$ ,  $Q^2$ , and  $W$ . The data show that the  $K^+\Sigma^0$  cross section falls more rapidly than the  $K^+\Lambda^0$  cross section as  $Q^2$  increases.

This paper reports measurements made at the Wilson Synchrotron Laboratory of the electroproduction of  $K^+$  mesons from a proton target.

In what is now standard notation,<sup>1</sup> electroproduction is treated as photoproduction by a virtual photon. The square of the proton's mass  $-Q^2$ , energy  $\nu$ , direction, and polarization  $\epsilon$  are tagged by the scattered electron. The hadronic cross section is a function of the virtual-photon variables and the variables describing the produced hadron in the virtual-photon-proton center-of-mass system,  $\theta^*$ ,  $\varphi$ , and  $(\text{MM})^2$ . The virtual photoproduction cross section can also be written in terms of the scaling variables  $x'$  and  $P_{\perp}^2$  defined in Bebek *et al.*<sup>2</sup> We have analyzed the inclusive data in terms of the cross-section differential in  $(\text{MM})^2$  and of the invariant structure function

$$F = \frac{E}{\sigma_{\text{tot}}} \frac{d^3\sigma}{dp^3} = \frac{1}{\sigma_{\text{tot}}} \frac{1}{\pi} \frac{E^*}{[P_{\text{max}}^{*2} - P_{\perp}^2]^{1/2}} \frac{d\sigma}{dx' dP_{\perp}^2}$$

Here  $\sigma_{\text{tot}}$  is the total virtual photoproduction cross section for the total energy  $W$  and  $Q^2$  of the

reaction. The value of  $\sigma_{\text{tot}}$  was taken from a fit to the Stanford Linear Accelerator Center-Massachusetts Institute of Technology measurements of  $\nu W_2$  made with the assumption  $\sigma_s/\sigma_T = 0.18$ .<sup>3</sup>

Two magnetic spectrometers were used to detect the scattered electron and the electroproduced hadron. The combination of a Cherenkov counter and a lead-acetate shower counter identified the electrons. Pions were identified by a threshold gas Cherenkov counter when their momentum was greater than 1.8  $\text{GeV}/c$  and by their time of flight when their momentum was less than that. Kaons were separated from protons by their time of flight.

Data were taken at the points in the  $(Q^2, \nu)$  plane shown in Fig. 1. Points 1, 3, and 7 comprise a  $Q^2$  scan at fixed  $W$ ; points 6 and 7 lie on the same  $\omega$  line and give a test of scaling; points 3 and 6 give a  $W$  scan at fixed  $Q^2$ ; and points 2, 4, and 5 give an angular scan with the hadron arm which extends the aperture in  $P_{\perp}$ . The acceptance of the apparatus is such that at each datum point the  $W$  distribution is approximately 0.6  $\text{GeV}$  wide and

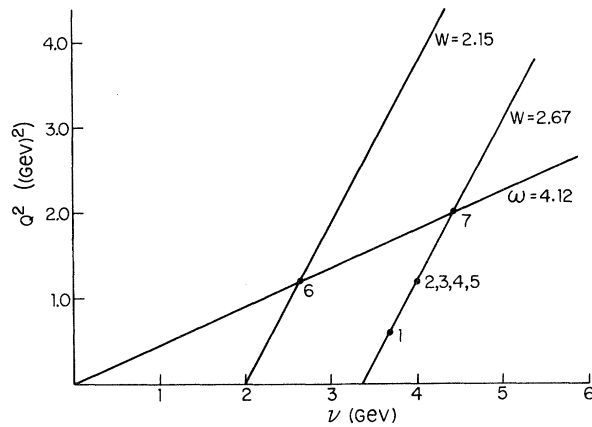


FIG. 1.  $Q^2, \nu$  plane showing the points at which data were taken.

the  $Q^2$  distribution about  $0.3 \text{ GeV}^2$  wide.

The data have been corrected for random coincidences ( $\approx 5\%$ ), counter and spark-chamber dead time ( $\approx 2\%$ ), absorption in the counters ( $\approx 2\%$ ), target-wall background ( $\approx 5\%$ ), and decay in flight (20 to 100%). The errors quoted are statistical; there is in addition a systematic uncertainty which is estimated to be less than 10%.

The  $(MM)^2$  distributions for the  $K^+$  at data points 1 and 7 are shown in Fig. 2. The peak around  $0.8 \text{ GeV}^2$  is due to elastic pions which failed to fire the Cherenkov counter and passed through the timing cuts; it was used to estimate the pion contamination in the  $\Lambda$ - $\Sigma^0$  region. The  $\Lambda$  peak is very prominent on both plots as is the peak at  $2.3 \text{ GeV}^2$  corresponding to the  $\Lambda(1520)$ . The  $\Sigma$  is clearly present at point 1 and is absent at point 7. The bump at  $1.9 \text{ GeV}^2$  is probably due to the  $\Sigma^0(1385)$  and/or the  $\Lambda(1405)$ .

The  $\Lambda$  and  $\Sigma^0$  cross sections were obtained by fitting the  $(MM)^2$  distributions with a curve constructed by folding a Gaussian resolution function with a radiative tail.<sup>4,5</sup> Table I summarizes the cross sections and the  $\Sigma^0/\Lambda$  ratio. Where they overlap the data are in good agreement with mea-

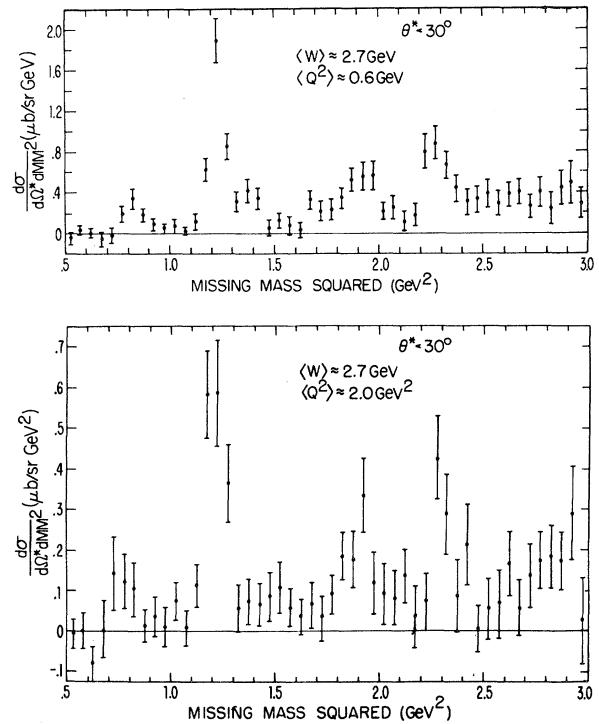


FIG. 2.  $(MM)^2$  distributions for a detected  $K^+$  at data points 1 and 7.

surements made at the Cambridge Electron Accelerator (CEA).<sup>6</sup> The most striking feature of the data is the low  $\Sigma^0/\Lambda$  ratio which always remains less than 0.25 and is consistent with zero at  $Q^2 = 2.0 \text{ GeV}^2$ . In photoproduction,  $\Sigma^0/\Lambda$  ratios are typically between 0.5 and 1.<sup>7</sup>

Figure 3 shows the  $Q^2$  dependence of the  $\Lambda$  and  $\Sigma$  cross sections for  $W \approx 2.65$ . Also shown are photoproduction data<sup>8</sup> and lower  $Q^2$  data from CEA<sup>6</sup> and a recent DESY experiment.<sup>9</sup> It is noteworthy that the  $\Lambda$  cross section falls less rapidly than  $1/Q^2$ . This is to be contrasted with the  $\pi^+n$  cross section which falls as  $1/Q^4$  in this region.

The dependence of the cross section on  $t' = t - t_{\min}$  was determined by a fit of the  $t'$  distribution with the form  $Ae^{Bt'}$ . The values of  $B$  in  $\text{GeV}^{-2}$

TABLE I. Summary of the fitted values of  $d\sigma/d\Omega^*$  for  $\Lambda$  and  $\Sigma^0$  for bins with  $0 \leq \theta^* < 15^\circ$ . Uncertainties include statistical and fitting errors.

| Point | $\langle W \rangle$<br>(GeV) | $\langle Q^2 \rangle$<br>( $\text{GeV}^2$ ) | $\langle \epsilon \rangle$ | $\langle \theta^* \rangle$<br>(deg) | $d\sigma(\Lambda)/d\Omega^*$<br>( $\mu\text{b}/\text{sr}$ ) | $d\sigma(\Sigma^0)/d\Omega^*$<br>( $\mu\text{b}/\text{sr}$ ) | $\Sigma^0/\Lambda$ |
|-------|------------------------------|---|----------------------------|-------------------------------------|---|--|--------------------|
| 1     | 2.67                         | 0.62  | 0.86                       | 7.77                                | $0.267 \pm 0.26$  | $0.035 \pm 0.015$  | $0.13 \pm 0.07$    |
| 2-4   | 2.66                         | 1.20  | 0.86                       | 8.42                                | $0.169 \pm 0.012$   | $0.038 \pm 0.008$  | $0.23 \pm 0.06$    |
| 7     | 2.66                         | 2.00  | 0.82                       | 7.45                                | $0.137 \pm 0.013$   | $0.006 \pm 0.006$  | $0.04 \pm 0.05$    |
| 6     | 2.20                         | 1.18  | 0.94                       | 7.44                                | $0.272 \pm 0.019$   | $0.035 \pm 0.012$  | $0.13 \pm 0.05$    |

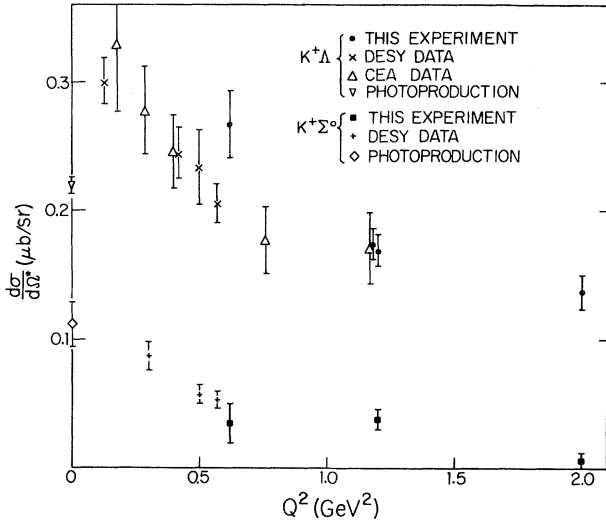


FIG. 3.  $Q^2$  dependence for the  $K^+\Lambda$  and  $K^+\Sigma^0$  cross sections. Also shown are photoproduction measurements (Ref. 8), measurements from a recent DESY experiment (Ref. 9), and measurements from CEA (Ref. 6). These latter measurements were all made at lower  $W \approx 2.2$  GeV and have been extrapolated to  $W = 2.66$  GeV by  $(W^2 - M_p^2)^{-1}$ .

at data points 1, 2-4, 6, and 7 were, respectively,  $6.5 \pm 4.3$ ,  $6.8 \pm 1.9$ ,  $6.2 \pm 2.6$ , and  $8.6 \pm 1.2$ .

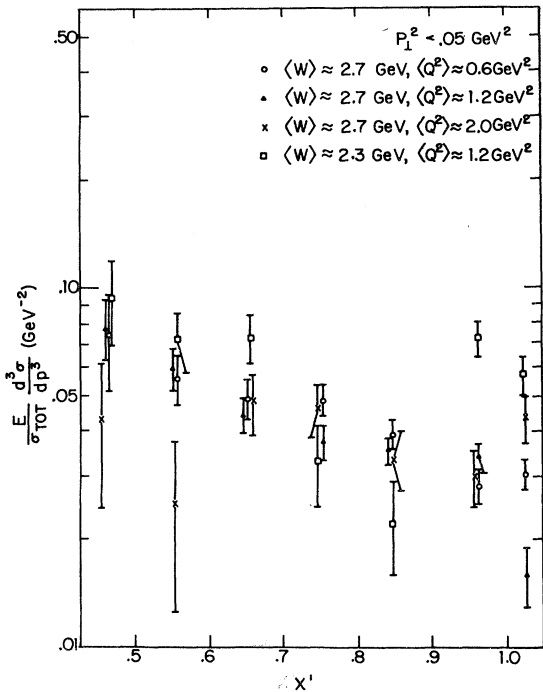


FIG. 4. Invariant structure function for kaons at data points 1, 2-4, 6, and 7.

TABLE II. Summary of the fitted cross sections for  $K^+\Lambda(1520)$  virtual photoproduction for bins with  $0 \leq \theta^* < 15^\circ$ . Uncertainties are statistical and fitting errors.

| Point | $\langle W \rangle$ (GeV) | $\langle Q^2 \rangle$ (GeV <sup>2</sup> ) | $\langle \epsilon \rangle$ | $\langle \theta^* \rangle$ (deg) | $d\sigma/d\Omega^*$ (μb/sr) |
|-------|---------------------------|---|----------------------------|----------------------------------|-----------------------------|
| 1     | 2.71                      | 0.61                                      | 0.86                       | 6.65                             | $0.127 \pm 0.016$           |
| 2-4   | 2.70                      | 1.18                                      | 0.85                       | 7.96                             | $0.081 \pm 0.013$           |
| 6     | 2.32                      | 1.14                                      | 0.92                       | 12.18                            | $0.094 \pm 0.031$           |
| 7     | 2.74                      | 1.94                                      | 0.80                       | 8.76                             | $0.067 \pm 0.018$           |

A similar procedure, with the addition of a linear background, was used to obtain cross sections for the  $\Lambda(1520)$ . The results are summarized in Table II.

Figure 4 shows the invariant structure function for  $P_{1^2} < 0.05$  GeV<sup>2</sup> for four values of  $W$  and  $Q^2$ . The data do not display a strong  $Q^2$  dependence and are inconclusive as to the  $W$  dependence. Figure 5 shows the ratio of the invariant structure functions for the  $K^+$  and the  $\pi^+$  at four values of  $W$  and  $Q^2$ . The most striking feature is the increase in the ratio as a function of  $Q^2$  for the largest  $x'$  points. This is due primarily to the decrease in the pion structure function in this region.<sup>2,10</sup>

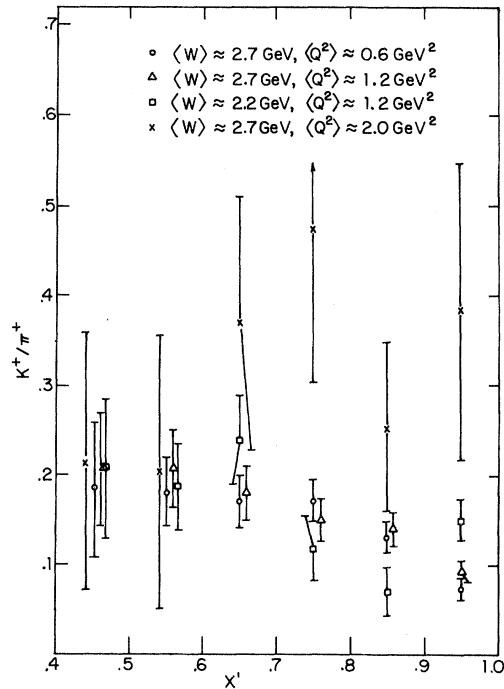


FIG. 5. Ratio of the invariant structure function for  $K^+$  and  $\pi^+$ . For the  $\pi^+$  data,  $0 \leq P_{1^2} < 0.02$  GeV<sup>2</sup>; for the  $K^+$  data,  $0 \leq P_{1^2} < 0.05$  GeV<sup>2</sup>.

We wish to acknowledge the support of the Director, Professor Boyce McDaniel, and the staff of the Wilson Synchrotron Laboratory. We also wish to acknowledge the support of the staff of the Harvard Cyclotron Laboratory.

\*Research supported in part by the U.S. Atomic Energy Commission and in part by the National Science Foundation.

†Present address: Physics Department, University of Rochester, Rochester, N.Y. 14627.

<sup>1</sup>K. Berkelman, in *Proceedings of the Sixteenth International Conference on High Energy Physics, The University of Chicago and National Accelerator Laboratory, Batavia, Illinois, 1972*, edited by J. D. Jackson and A. Roberts (National Accelerator Laboratory, Batavia,

Ill., 1973), Vol. 4, p. 41; L. N. Hand, *Phys. Rev.* **129**, 1834 (1964).

<sup>2</sup>C. J. Bebek *et al.*, *Phys. Rev. Lett.* **30**, 624 (1973).

<sup>3</sup>W. B. Atwood, private communication.

<sup>4</sup>A. Bartl and P. Urban, *Acta Phys. Austr.* **24**, 139 (1966).

<sup>5</sup>L. W. Mo and Y. S. Tsai, *Rev. Mod. Phys.* **41**, 205 (1969).

<sup>6</sup>C. N. Brown *et al.*, *Phys. Rev. Lett.* **28**, 1086 (1972).

<sup>7</sup>R. Erbe *et al.*, *Phys. Rev.* **188**, 2060 (1969).

<sup>8</sup>P. Feller *et al.*, paper submitted to the Sixth International Symposium on Electron and Photon Interactions at High Energies, Bonn, Germany, 27–31 August 1973 (to be published).

<sup>9</sup>T. Azemoon *et al.*, paper submitted to the Sixth International Symposium on Electron and Photon Interactions at High Energies, Bonn, Germany, 27–31 August 1973 (to be published).

<sup>10</sup>C. J. Bebek *et al.*, to be published.

## Production of Large-Transverse-Momentum Gamma Rays in $pp$ Collisions from 50 to 400 GeV

D. C. Carey, M. Goldberg,\* J. R. Johnson, D. J. Ritchie, A. Roberts, R. Shafer, D. Theriot, E. von Goeler,† J. K. Walker, and M. Wong‡  
National Accelerator Laboratory, Batavia, Illinois 60510

and

F. E. Taylor  
Northern Illinois University, DeKalb, Illinois 60115  
(Received 8 October 1973)

We have measured  $d^2\sigma_\gamma/dk d\Omega$  for the reaction  $p+p \rightarrow \gamma + \text{anything}$  at incident proton energies from 50 to 400 GeV. The experiment was performed in the National Accelerator Laboratory internal target area, using a lead-glass total-absorption counter. The cross sections show a deviation from simple exponential behavior in  $p_t$  for incident proton energies above 50 GeV and  $p_t$  greater than about 1 GeV/c. We present preliminary results on the energy dependence of this effect.

The behavior of cross sections for processes occurring with large transverse momentum is currently of considerable interest. In particular, measurements of inclusive pion production at the CERN intersecting storage rings (ISR)<sup>1-3</sup> have exhibited at large  $p_t$  a strong enhancement over the simple exponential falloff found at small  $p_t$  ( $<1$  GeV/c). We have studied the process  $p+p \rightarrow \gamma + \text{anything}$  in the range of  $p_t$  from about 0.2 to 3 GeV/c for incident proton energies from 50 to 400 GeV. Using the method of Sternheimer<sup>4</sup> and assuming all the observed photons come from  $\pi^0$  decay, the invariant  $\pi^0$  cross sections can be derived from these measurements.

The experiment was carried out in the  $C_0$  straight section of the National Accelerator Laboratory (NAL) main ring, using the circulating

proton beam incident on a thin internal target. Thus, data could be taken over the range of proton energies available during the accelerator cycle. Figure 1 shows the layout of the apparatus in the internal target area and a schematic of the detection system. The target was either a hydrogen gas jet<sup>5,6</sup> or 7- $\mu\text{m}$  carbon fibers on a rotating wheel. For the data presented here, the apparatus was set at a lab angle of 100 mrad with respect to the beam direction. Permanent magnets were used to sweep away low-momentum charged particles. A lead collimator prevented the apparatus from detecting both photons from the decay of  $\pi^0$ s with transverse momenta in the range studied.

The detection system consisted of a veto counter (No. 1), a removable lead converter (1.1 radi-